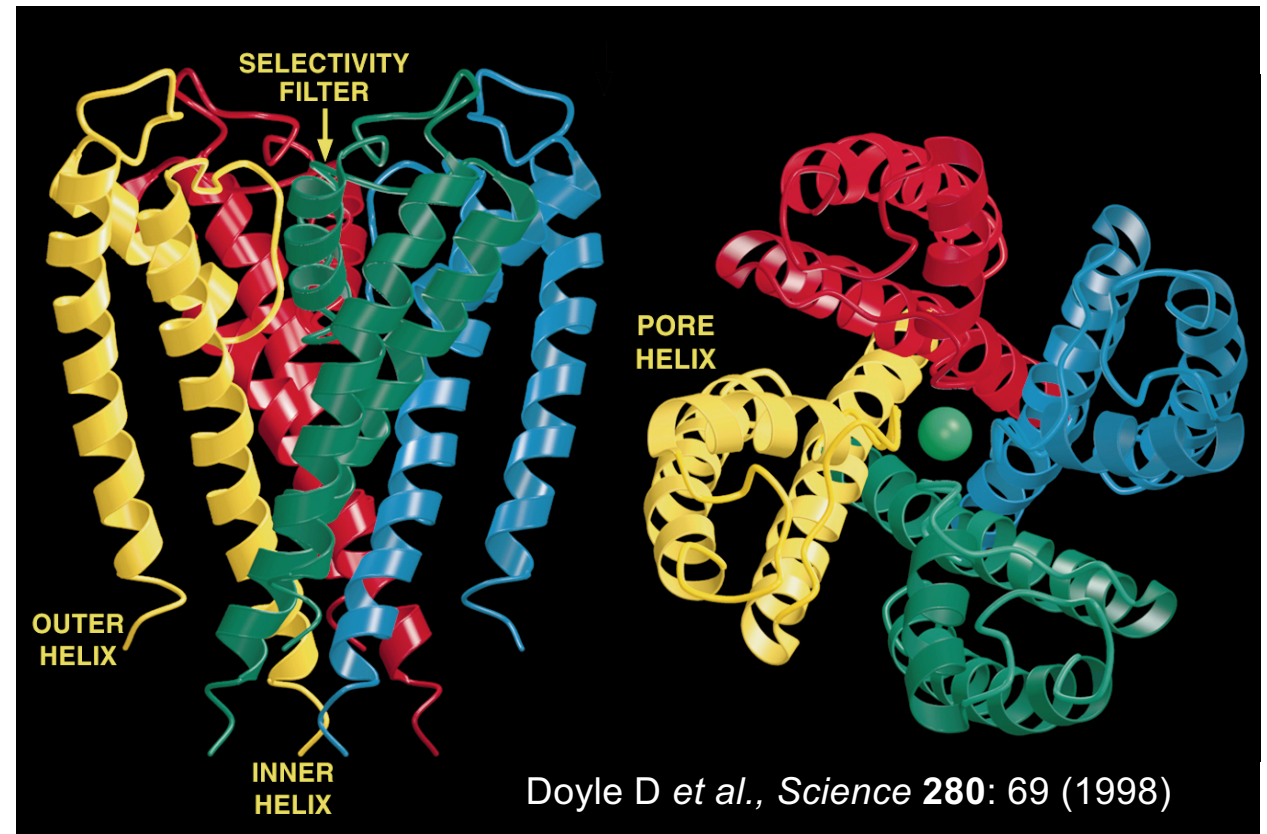


K⁺ channels

- Ubiquitous protein superfamily
- Tetramers with single, central ion conduction pathway
- ~10⁷-10⁸ K⁺ ions / sec per channel protein
- Selectivity:
K⁺ > Rb⁺ > Cs⁺ >> Li⁺ > Na⁺

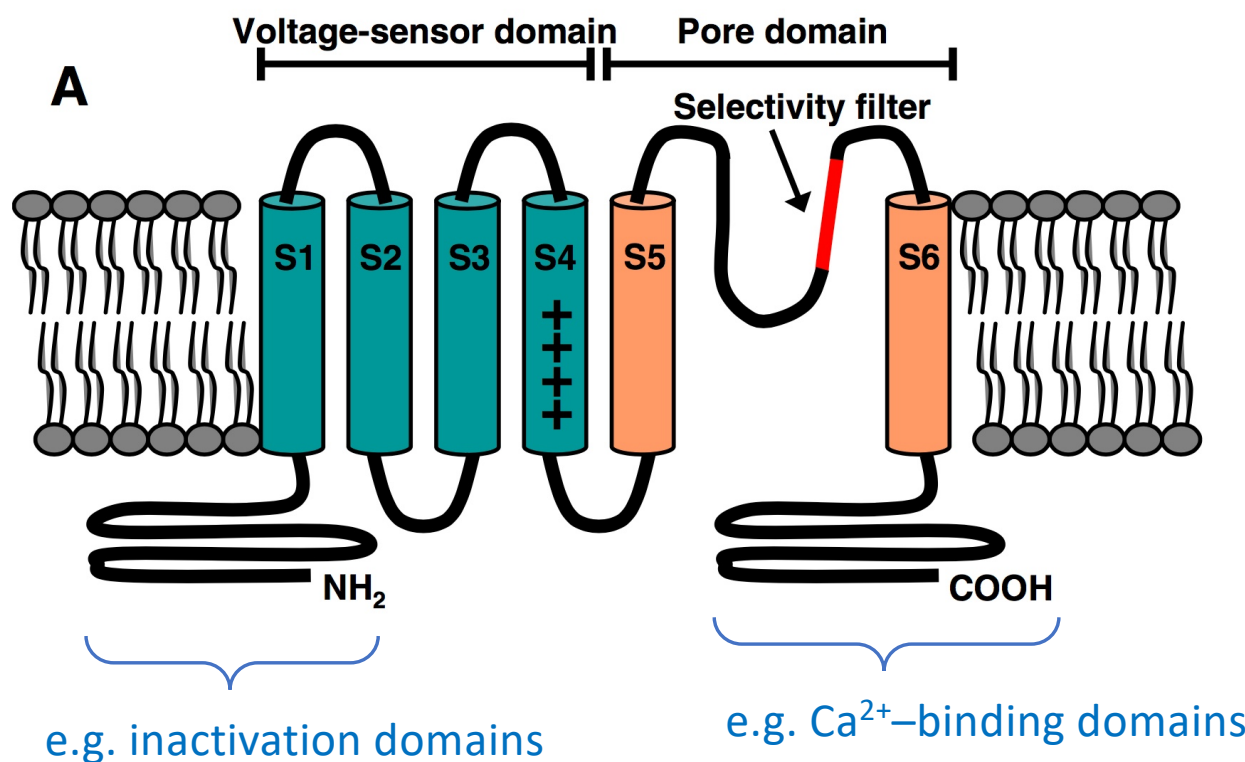
- P_{K⁺} : P_{Na⁺} ≈ 1000 (permeability)

Structure of *Streptococcus lividans*
KcsA (bacterial K⁺ channel homologue).

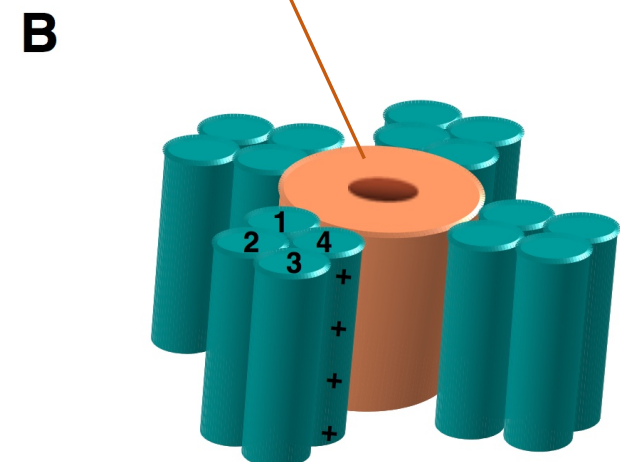


Roderick MacKinnon

K⁺ channel topology / architecture



Minimal channel domain / core



Borjesson SI et al., *Cell Biochem Biophys* 52: 149-174 (2008)

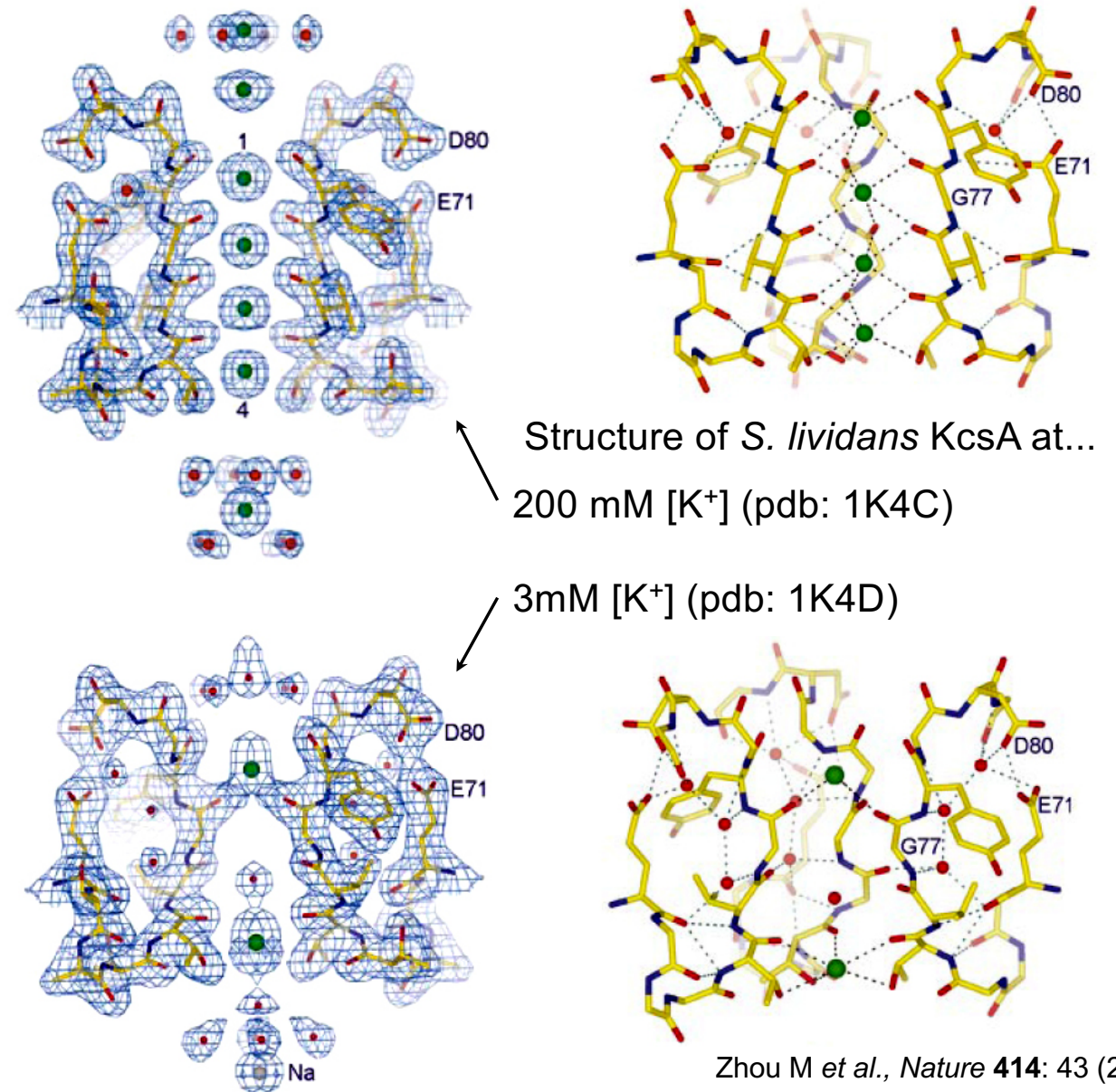
pymol KcsA high res high K+

PDB ID: 1K4C.pdb

- Pymol scene 1: Ribbon
- Pymol scene 2: Fab-KcsA monomer complex
- Pymol scene 3: Fab-KcsA crystallographic symmetry to tetramer
- Pymol scene 4: Sticks, top view into K conduction pore
- Pymol scene 5: Side view of conduction pore, one KcsA monomer cut for clarity
- Pymol scene 6: Same as 5 but with VdW spheres for K ions built in selectivity filter
- Pymol scene 7: K in dehydration chamber

Selectivity filter

- Central pathway: backbone C=O of pore loop provide ligands to 4 well-defined ion binding pockets
- At high $[K^+]$ (200 mM), each potassium ion has 8 potential oxygen ligands (similar to hydration with H_2O in solution)
- Binding affinities of K^+ ions low (explaining high conductance rates!). This is known from determining structures at lower K^+ concentrations (3 mM)
- At 3 mM potassium, not all 4 sites are occupied by K^+ and the selectivity filter has partially collapsed.



S. lividans KcsA: K⁺ conductance at physiological [K⁺]

Adjacent peaks in the K⁺ electron density profile are separated by about 3.2 Å (Fig. 3b). Potassium ions have a diameter of 2.7 Å, so they could, in principle, fit in the filter side by side, but this would seem to be an unstable binding configuration for electrostatic reasons. A survey of a database of small-molecule structure (Cambridge Crystallographic Data Centre, <http://www.ccdc.cam.ac.uk>) showed us that two K⁺ ions only very rarely occur with a separation distance of less than 3.5 Å. Therefore, although K⁺ ions may in principle occupy adjacent sites in the selectivity filter, we expect that most often they are separated by an intervening water molecule.

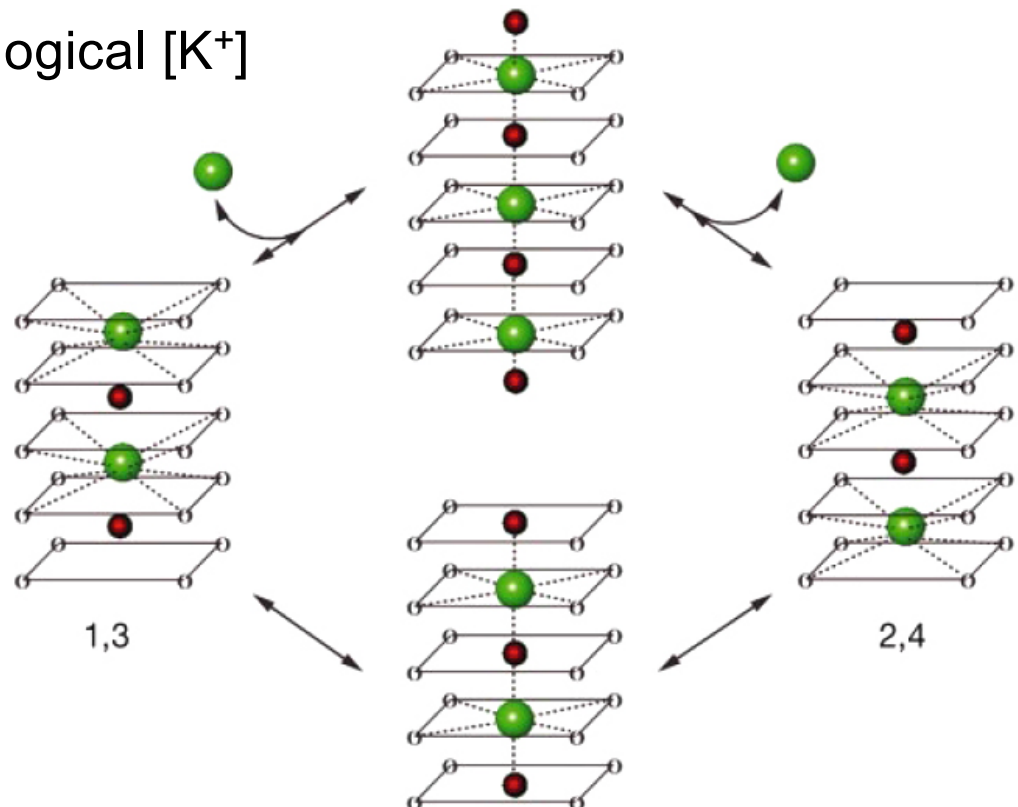
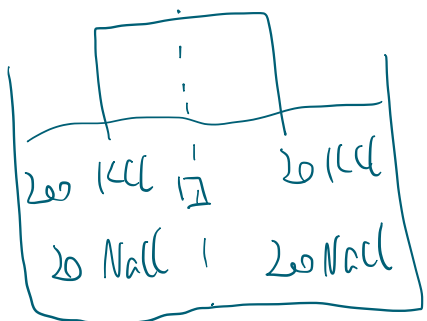
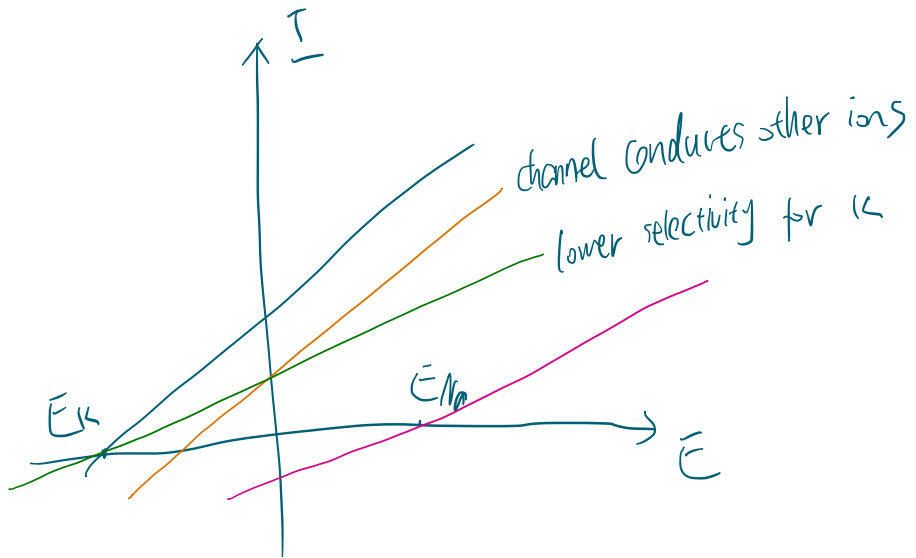


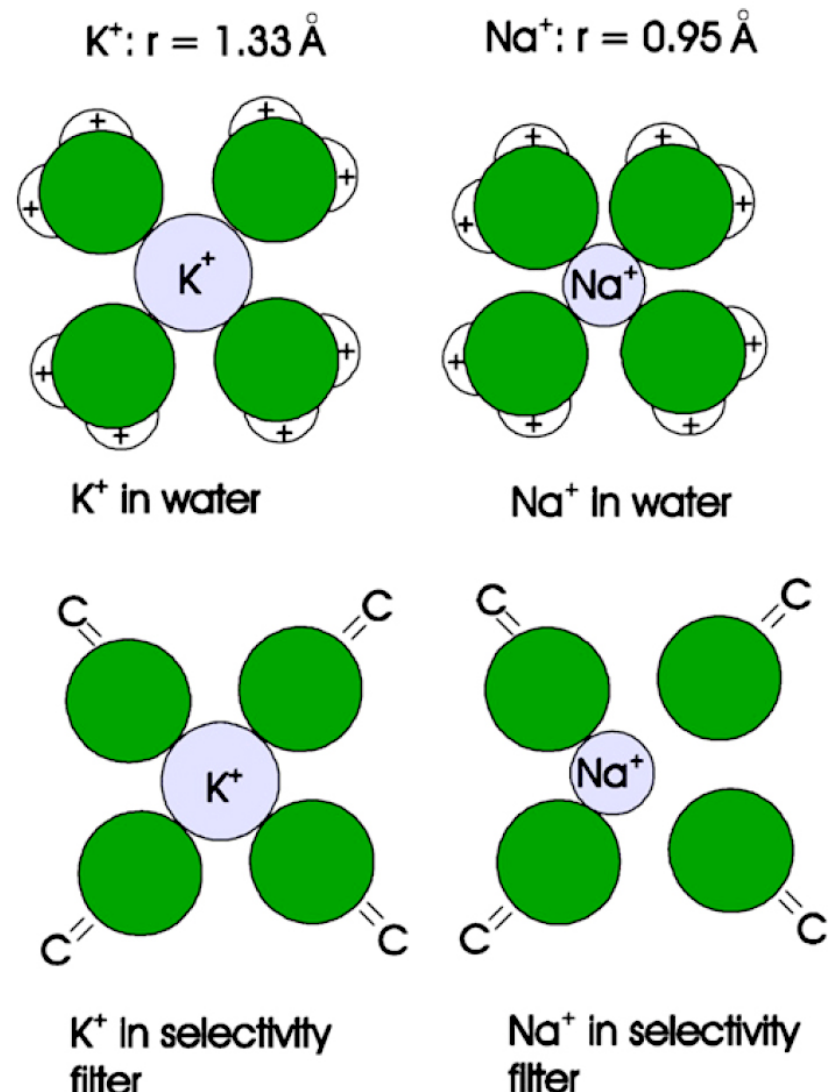
Figure 5 The biologically important throughput cycle for K⁺ ions. **a**, Detailed description of the cycle connecting states B and C (Fig. 4a). The selectivity filter is depicted as five sets of four in-plane oxygen atoms (the top is outside the cell), with K⁺ ions and water molecules shown as green and red spheres, respectively. K⁺ ions undergo coordination by eight oxygen atoms when in the 1,3 and 2,4 configurations. Movement along either the concentration-independent path (bottom) or the concentration-dependent path (top) would involve octahedral coordination by six oxygen atoms, two provided by the intervening water molecules.

Selectivity measurements (blackboard)



Selectivity: K⁺ vs. Na⁺ hydration in water and K⁺-channel selectivity filter.

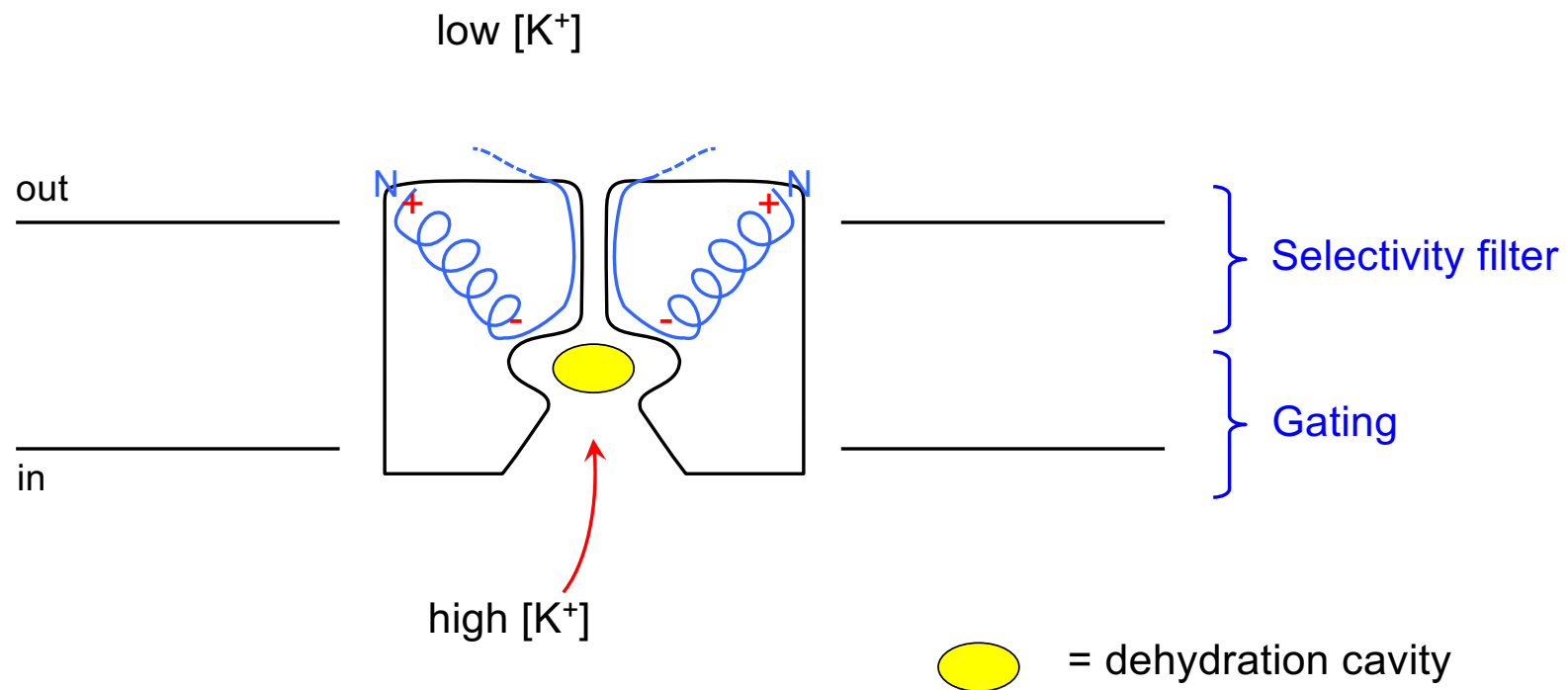
Fig. 4. A model for K⁺-Na⁺ discrimination by the filter (13). A K⁺ ion (1.33 Å crystal radius) in the selectivity filter has about the same energy as in water and is bound to either oxygens of water molecules or carbonyl oxygens in the pore. The carbonyl groups have higher dipole moments than the water molecules, which helps to overcome the image forces that arise from the low dielectric constant of the membrane (54). An Na⁺ ion (0.95 Å crystal radius) in the filter has higher energy than one in water, because it binds effectively to only two of the four carbonyls shown. The other two carbonyls are prevented from collapsing around the Na⁺ ion by structural constraints in the filter wall.



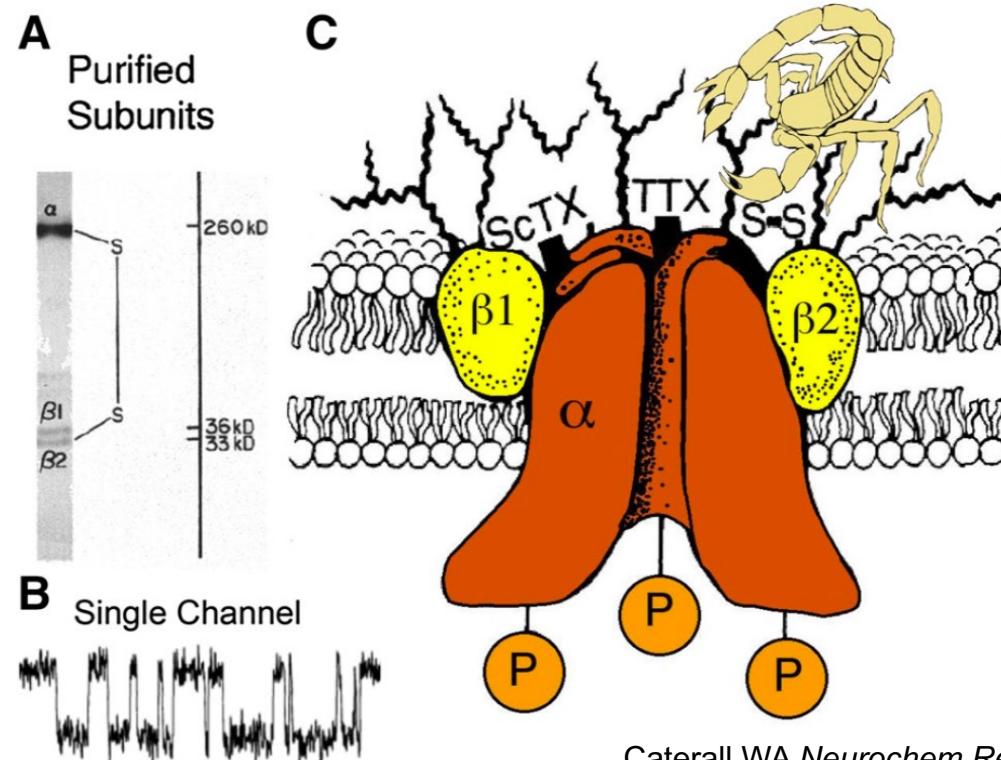
Armstrong CM et al., *Science Signaling* Vol. 2003, Issue 188, pp. re10

Conclusion: Coordination / size mismatch of Na⁺ vs K⁺ in K⁺ channel selectivity filter ("snug fit" of K⁺ ions)

Summary K⁺ channel selectivity / conductance features



Na⁺ channels



William Catterall

Catterall WA *Neurochem Res* **42**: 2495-2504 (2017)

- A. Sodium channels as originally purified from mammalian brain. The α and $\beta 1$ subunits of brain sodium channels analyzed by SDS-PAGE.
- B. Single channel currents from purified and reconstituted brain sodium channels.
- C. A model of the rat brain sodium channel derived from biochemical experiments. This model depicts the state of the field in 1986 when it was drawn.

Na^+ channels

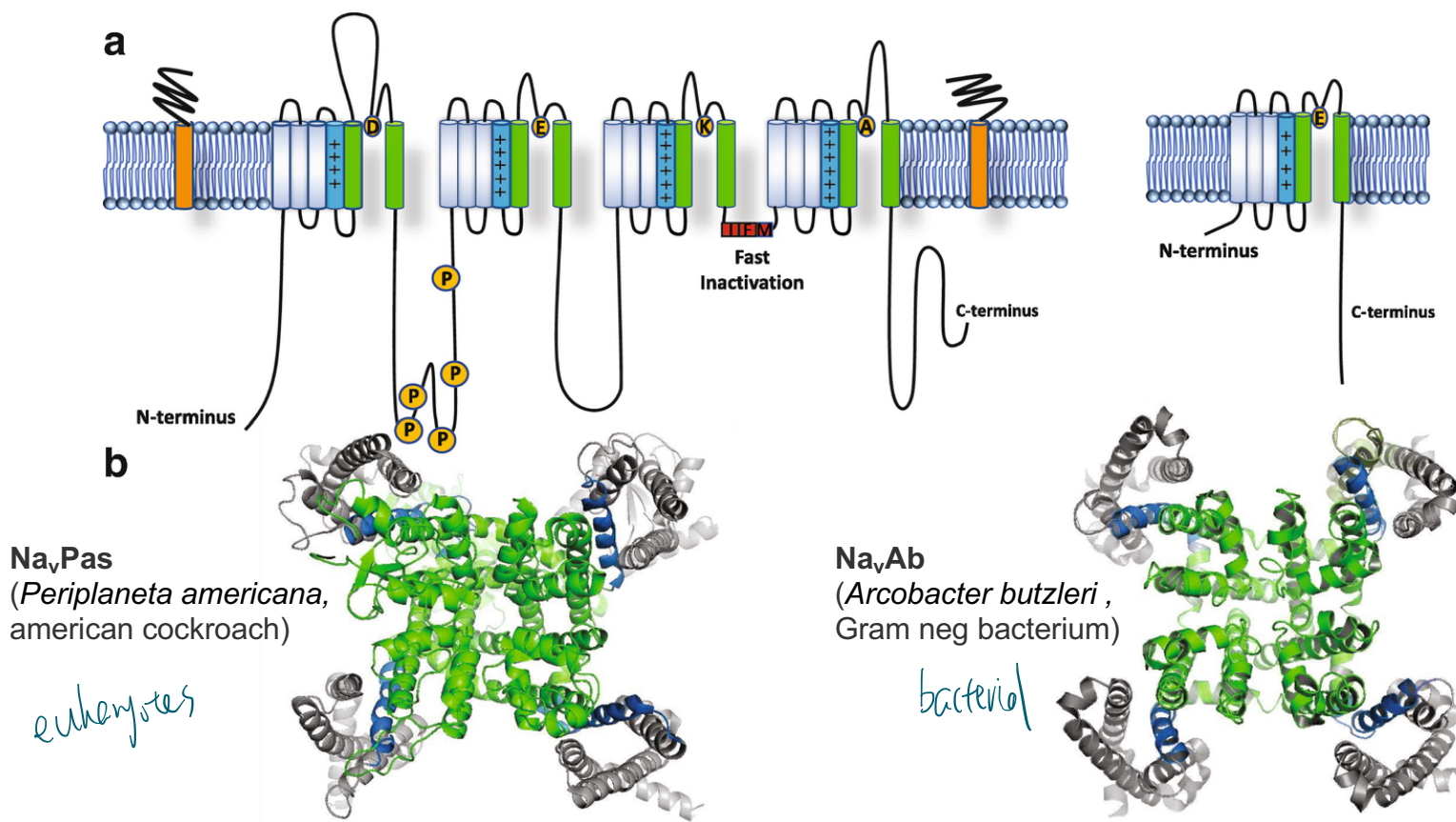
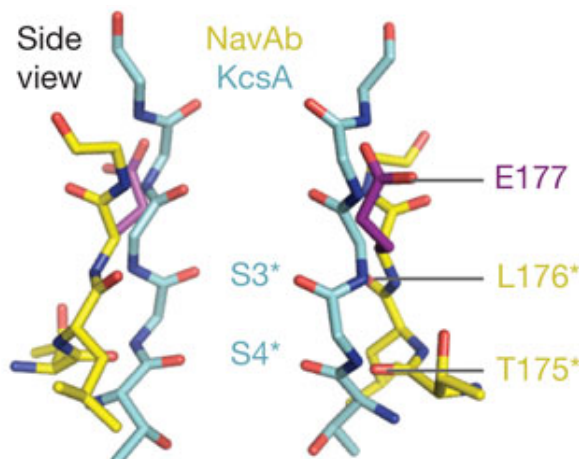
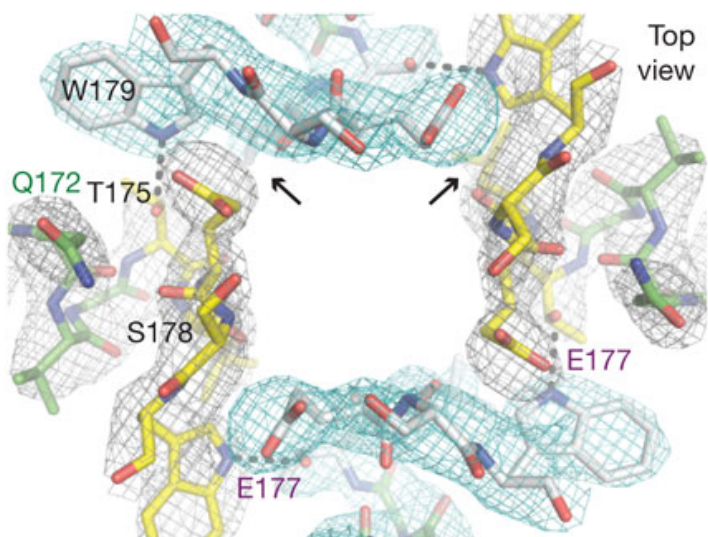
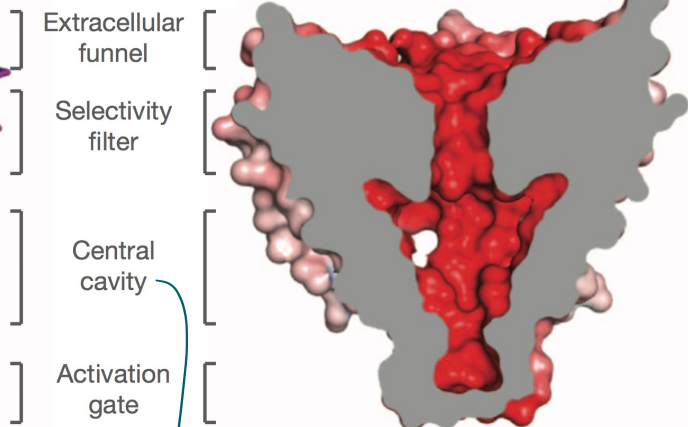
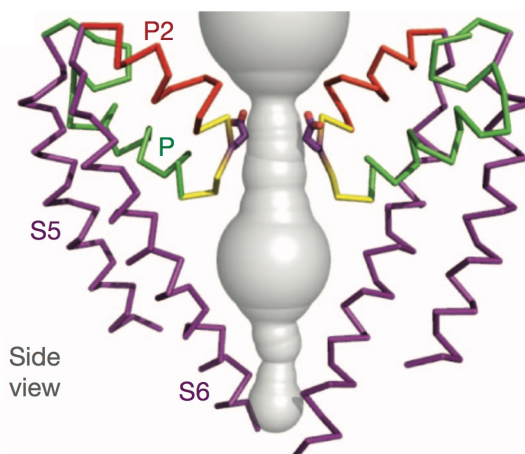
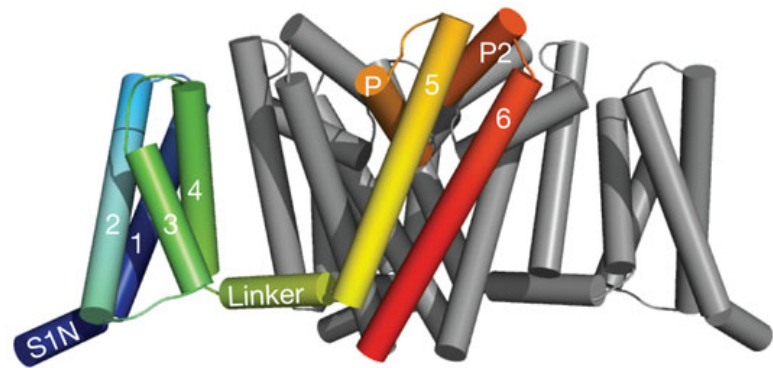


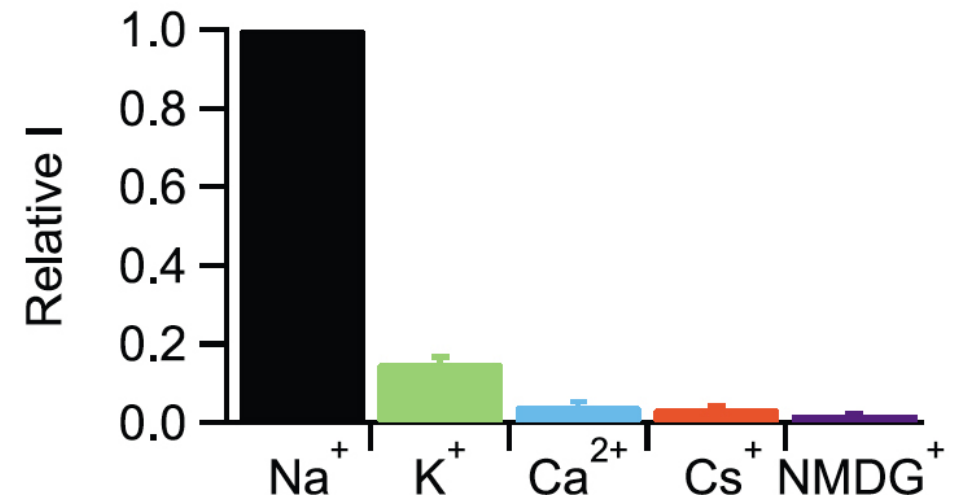
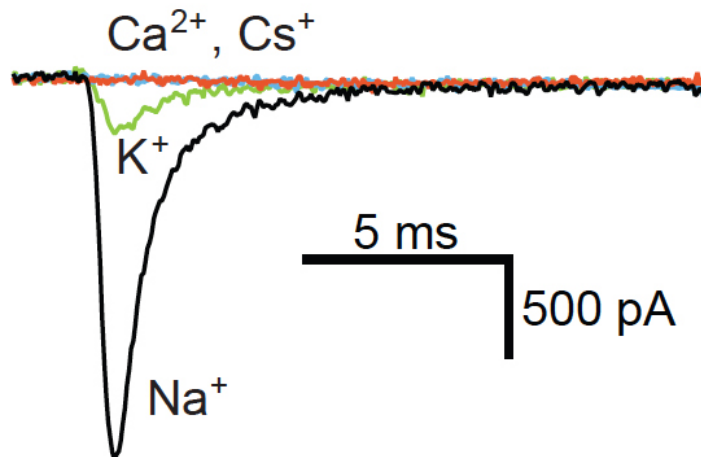
Fig. 1 Overall structures of eukaryotic and prokaryotic sodium channels. **(a)** Topology of a eukaryotic voltage-gated sodium channel showing four homologous domains. Each domain consists of six segments. Voltage-sensing segments (S1–S4) are shown in gray with S4 segment depicted in *marine blue*. The pore domain (S5–S6) is shown in *light green*. **(b)** *Top view* of the overall model of the eukaryotic voltage-gated sodium channel NavPas (*left*) (5X0M) and bacterial sodium channel NavAb (*right*) (PDB 3RVZ). Key structural and functional features of Na_vPas (*left*) and Na_vAb (*right*) channels are color labeled including the voltage sensor domain (S1–S3, *green*; S4, *marine blue*), pore domain (*light green*)

Arcobacter butzleri voltage-gated Na⁺ channel (Na_vAb) at 2.7 Å resolution



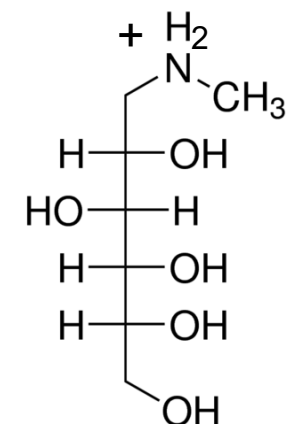
Payandeh J et al. *Nature* **475**: 353-358 (2011)

Electrophysiological characterization of $\text{Na}_\text{v} \text{Ab}$



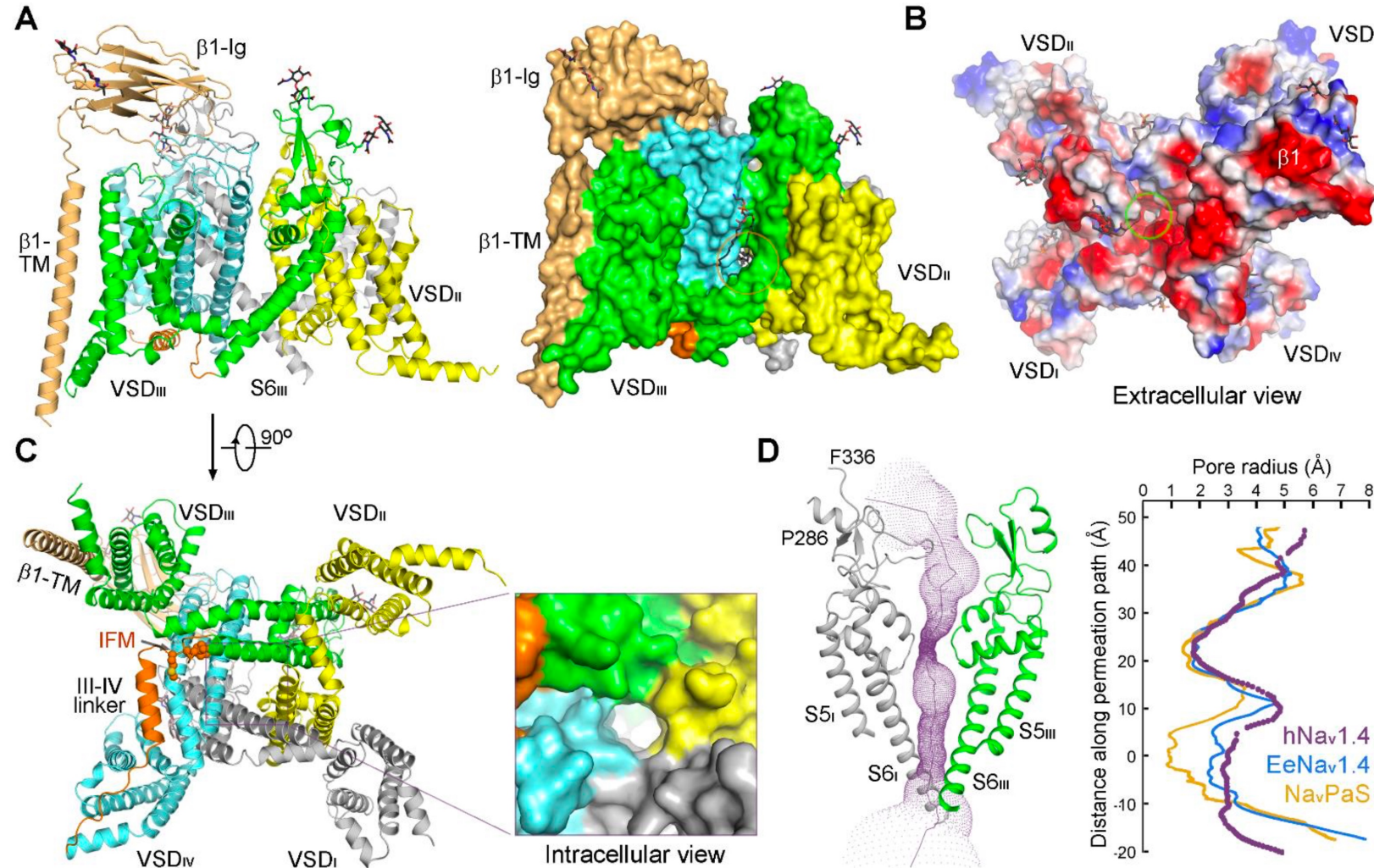
NavAb current traces obtained in a cell exposed sequentially to Na^+ -containing, K^+ -containing, Cs^+ -containing and Ca^{2+} -containing solutions during depolarizations to 20 mV from a holding potential of -120 mV.

NMDG = N-methyl-D-glucamin



Na^+ channels are very similar while Ca^+ channels are more different

Cryo-EM and the tsunami of channel structures



Nieng Yan

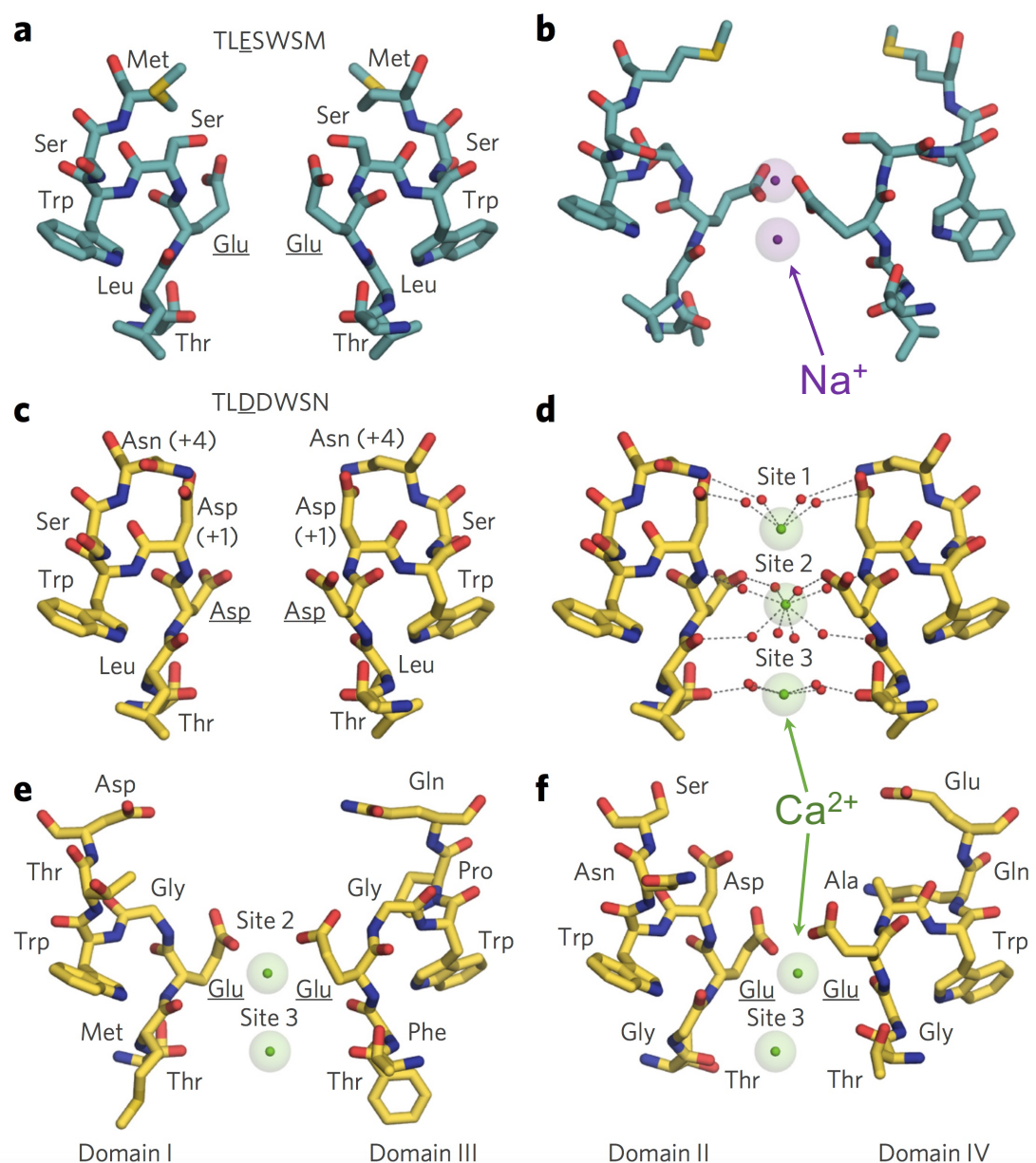


Yifan Cheng

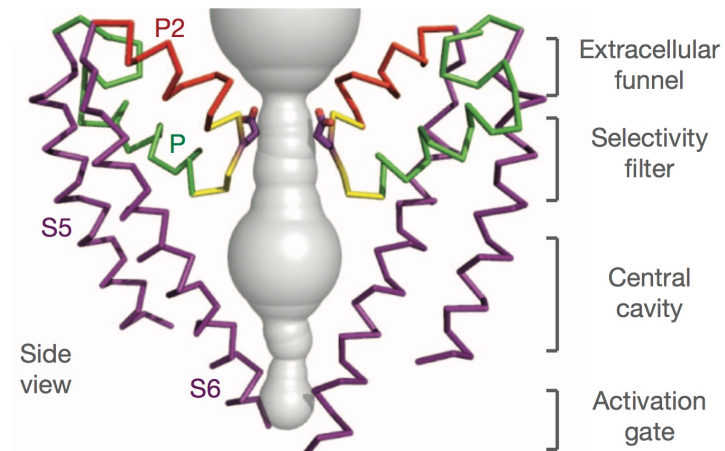
Pan X et al. *Science* **362**: 6412 (2018), see also Shen H et al., *Science* **355**: 6328 (2017)

Ion permeation and selectivity of NaV and CaV channels.

Figure 5 | Chemical mechanism of ion permeation and selectivity of Na_v and Ca_v channels with structural models of their ion selectivity filters with ions bound. (a) Na⁺ selectivity filter (TLESWSM) in Na_vAb. (b) Representative conformations of Na⁺ selectivity filter from molecular dynamic simulations of sodium permeation in Na_vAb. Conformational dunking of the Glu side chain of the high-field-strength site allows direct coordination of Na⁺ ions. (c) Ca²⁺ selectivity filter (TLDDSN) in Ca_vAb. (d) Hydrated Ca²⁺ bound in the Ca_vAb selectivity filter. (e) Ca²⁺ selectivity filter of Ca_v1.1 from domains I (TMEGWTD) and III (TFEGWPQ). (f) Ca²⁺ selectivity filter of Ca_v1.1 from domains II (TGEDWNS) and IV (TGEAWQE). Na⁺ (purple) and Ca²⁺ (green) ions are shown with semitransparent ionic sphere. Dashed lines indicate network of interactions among coordinated water molecules with the ions and protein atoms from high-filled strength site (Glu in Na_vAb and Ca_v1.1, and Asp in Ca_vAb, underlined) and backbone carbonyls of Leu and Thr. For clarity, only two opposing subunits in the tetramer are shown.



Ion permeation and selectivity of NaV and CaV channels.



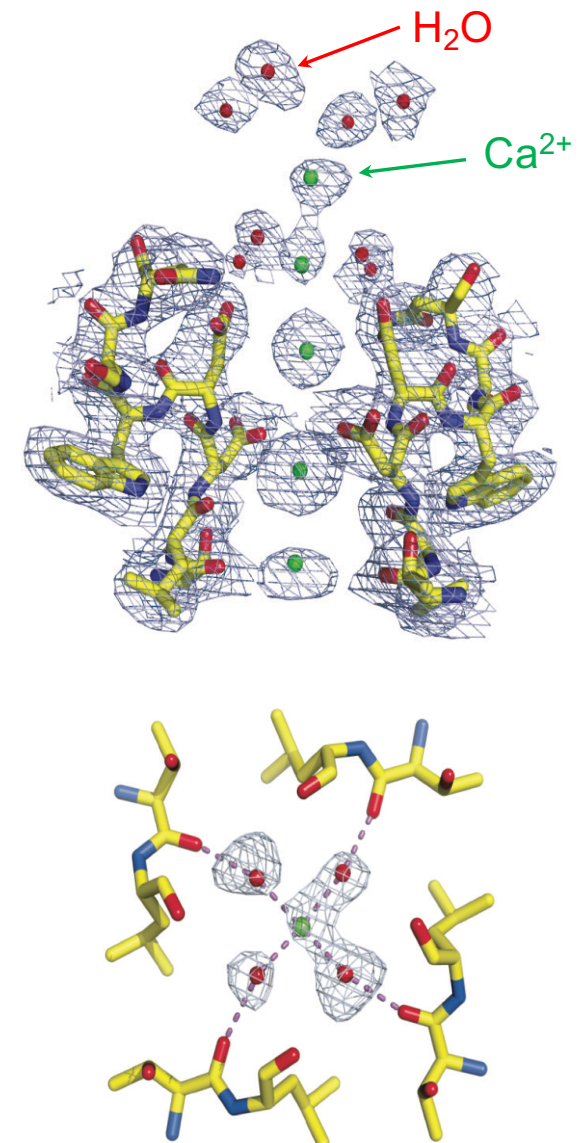
2.5. Sodium Conductance and Selectivity

As for voltage-gated potassium channels, sodium conductance and selectivity are mediated by the P loops in the four pore-forming modules of sodium channels (**Figure 1e**), which interact with Na^+ as it approaches and enters the ion selectivity filter (25, 52–55). However, in sharp contrast to potassium channels, the outward-facing edge of the ion selectivity filter is composed of a square array of four glutamate (Glu) residues in bacterial Na_V channels (25) or an array of four different amino acid residues, Asp-Glu-Lys-Ala, in metazoan Na_V channels (32). This high field-strength site partially dehydrates the approaching Na^+ ion and allows only Na^+ to pass efficiently (52–54). Unexpectedly, the side chains of the Glu residues at the high field-strength site move inward with each Na^+ by rotating at a single torsion angle in a **dunking motion** that takes place at the rate of Na^+ permeation, $>10^7$ per second (52, 56). This dunking motion allows Na^+ to be conducted in a degenerate set of partially dehydrated complexes with the Glu side chains and increases the rate of Na^+ conductance.

Ion permeation and selectivity of NaV and CaV channels.

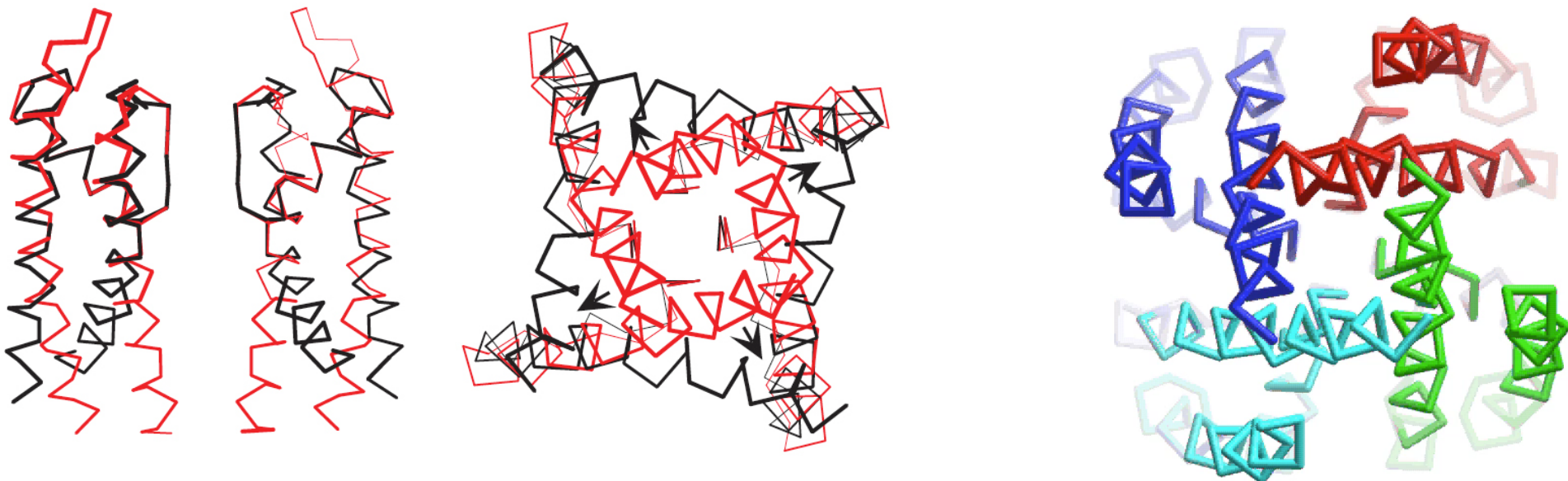
2.6. Calcium Selectivity

Vertebrate Cav channels have an ion selectivity filter with a high field-strength site containing four Glu residues, similar to NavAb and the other bacterial sodium channels (24, 55). These residues are crucial for calcium selectivity and conductance in eukaryotic calcium channels (55). The addition of negatively charged residues in the outer vestibule of NavAb, following the pattern in eukaryotic calcium channels (57), converts NavAb to a form with high calcium selectivity, designated CavAb (58). Determination of the structure of CavAb by X-ray crystallography revealed a series of closely spaced Ca^{2+} binding sites at approximately 4-Å intersite intervals that lead through the ion selectivity filter (58) (Figure 2c). These sites are occupied sequentially by Ca^{2+} as it moves inward through the pore. Like Na^+ , Ca^{2+} is conducted as a hydrated cation, and waters of hydration can be resolved in favorable crystal structures (58) (Figure 2c). As originally proposed in biophysical models of Ca^{2+} permeation (59–61), these sites bind Ca^{2+} with high affinity in order to prevent monovalent cation permeation, and yet they give high conductance of Ca^{2+} by the knock-off effect of electrostatic repulsion of one entering Ca^{2+} on the preceding Ca^{2+} ions in the pore (58). Consistent with the requirement for a series of Ca^{2+} -binding sites for conductance, Cd^{2+} binds to a single site and blocks the pore but is not conducted (58) (Figure 2c).



K⁺ channels: Comparison of open and **closed** conformations.

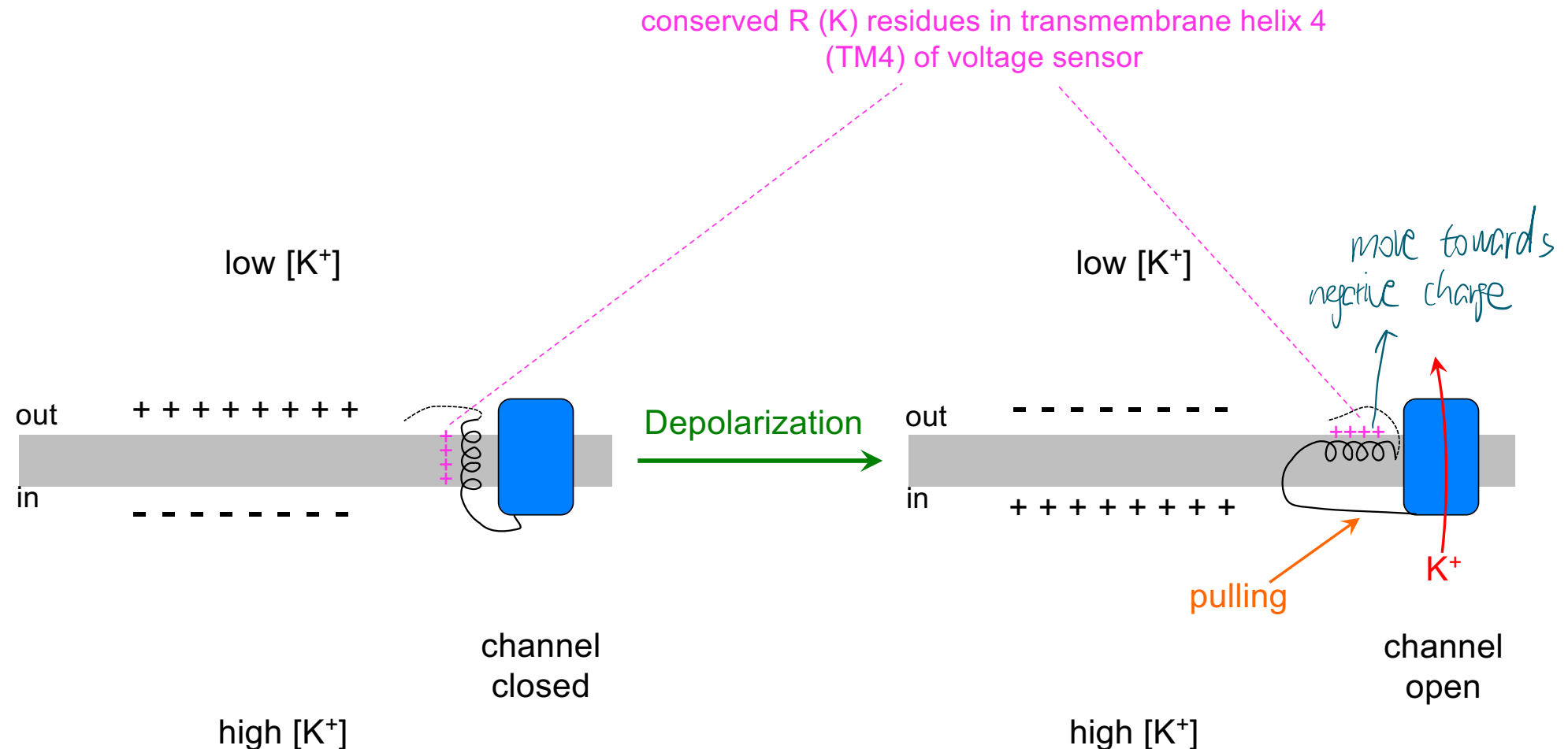
- Gating: Conformational change of cytoplasmic ends of inner helices (TM6). This opens or constricts the entrance to the channel pore.
- The "pulling apart" of TM6 can occur via C-terminal domains or via the cytoplasmic end of TM5 being pulled (e.g. by TM4 in voltage-gated channels)
- The conformation of the selectivity filter region remains unchanged.



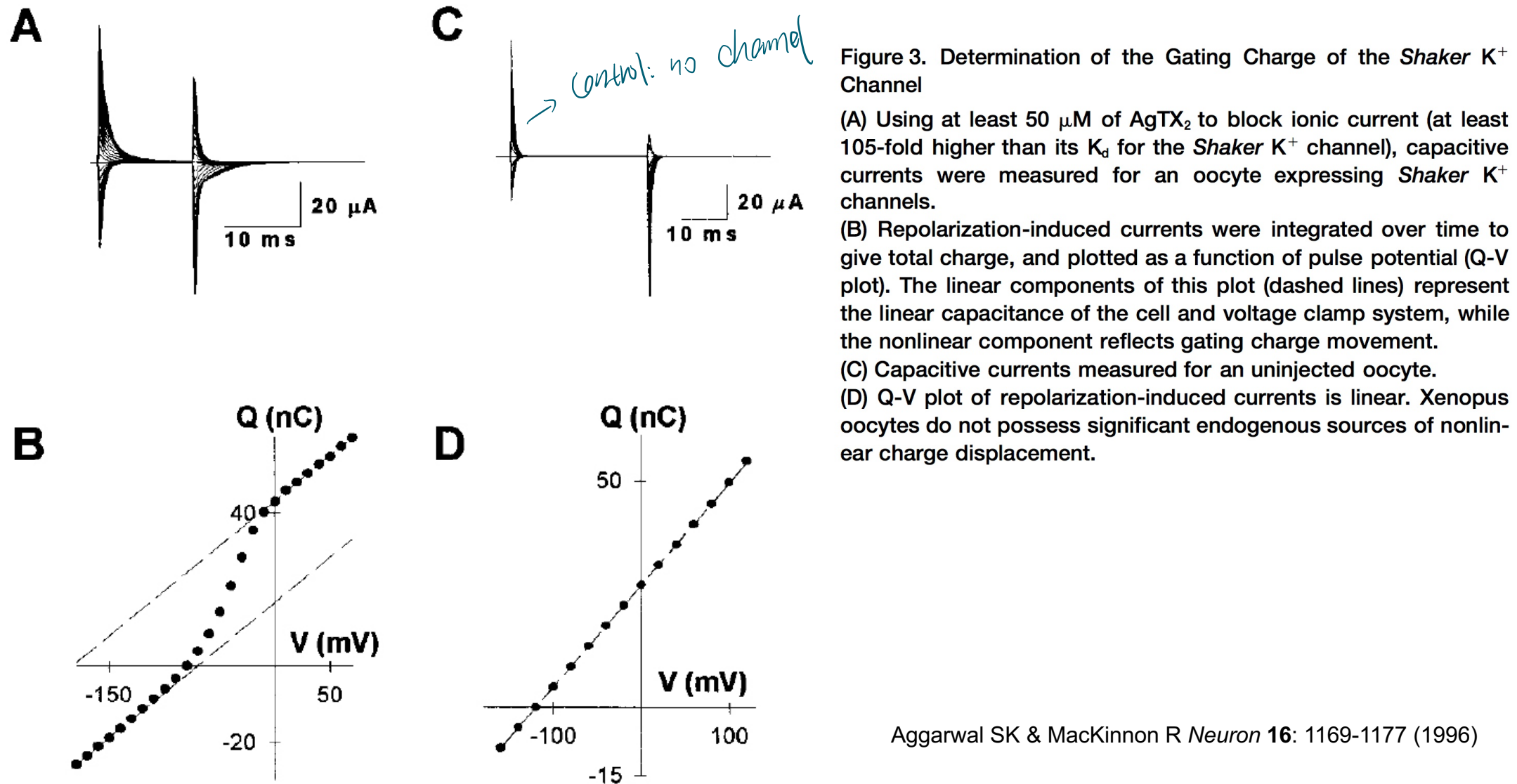
Jiang Y et al., *Nature* 417: 523 (2002)

K^+ channels: Voltage gating requires gating charges

(The schematic is simplistic and, with respect to detailed motions, incorrect)



Capacitive currents of Shaker K⁺ channel measured in the presence of agitoxin.

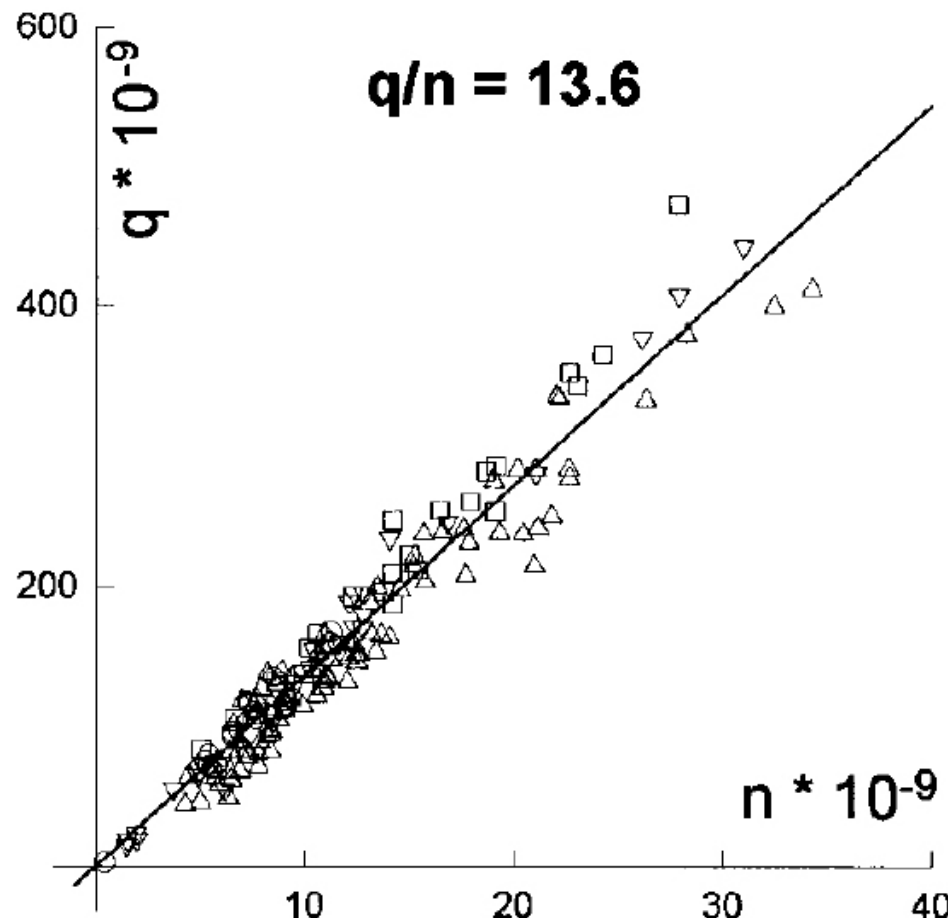


Aggarwal SK & MacKinnon R *Neuron* 16: 1169-1177 (1996)

Gating charges / current

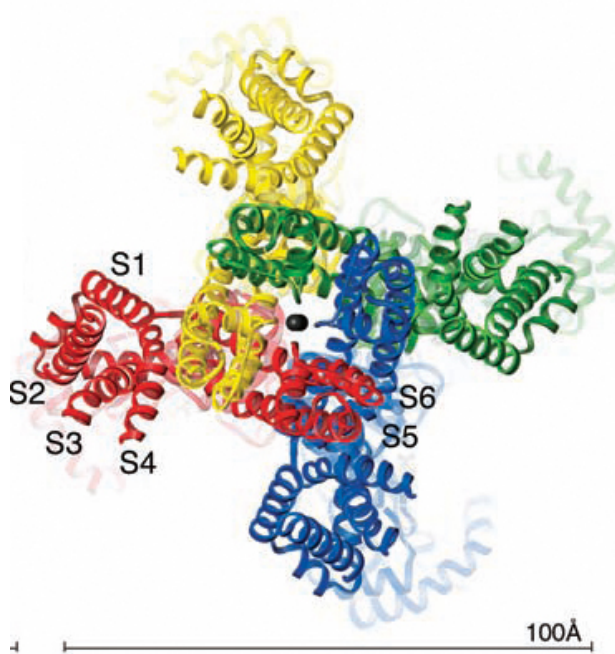
Integration of capacitive currents over time yields number of charges moved

E



(E) Correlation plot mapping total gating charge (q) in electron charge units as a function of total channel number (n) for several oocytes expressing *Shaker K⁺* channels. Total channel number was determined by binding oocytes with 85 nM tritiated AgTX₁D20C. Each point represents a different oocyte ($n = 162$), and each set of symbols (circles, squares, triangles, and inverted triangles) represent measurements made with independent radiolabeled toxin preparations. The line corresponds to a linear regression fit using the methods of least squares with a slope, or charge per channel (q/n), of 13.6 electron charge units. The 95% confidence interval for this measurement is ± 0.2 electron charge units.

Debate on the structural mechanism of voltage gating: Pistons, paddles, and rotating helices



Long et al., *Science* **309**: 897 (2005)

Jiang et al., *Nature* **423**: 33 (2003)

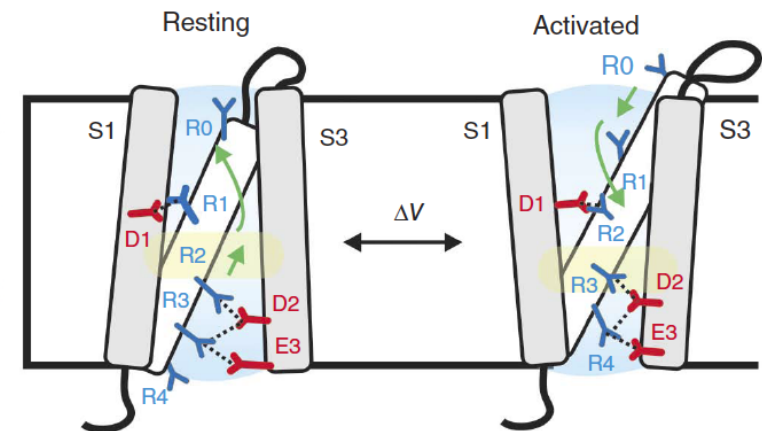
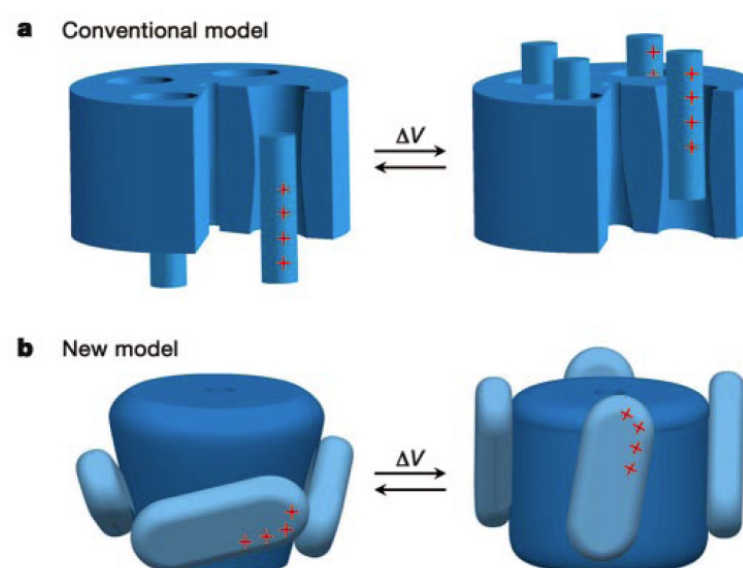


Fig. 6 (e) Mechanistic model of voltage sensing in Ci-VSD. An ~5-Å downward movement of S4 is accompanied by a counterclockwise ~60° rotation of the entire helix. Arginines in S4 are stabilized by successive negative countercharges on S1 and S3. A potential rotameric reorientation of the arginines might additionally contribute to the overall gating-charge transfer.

Li et al., *Nat Struct Mol Biol* 21: 244 (2014)

Mechanosensitive channels: Functional characterization



Boris Martinac

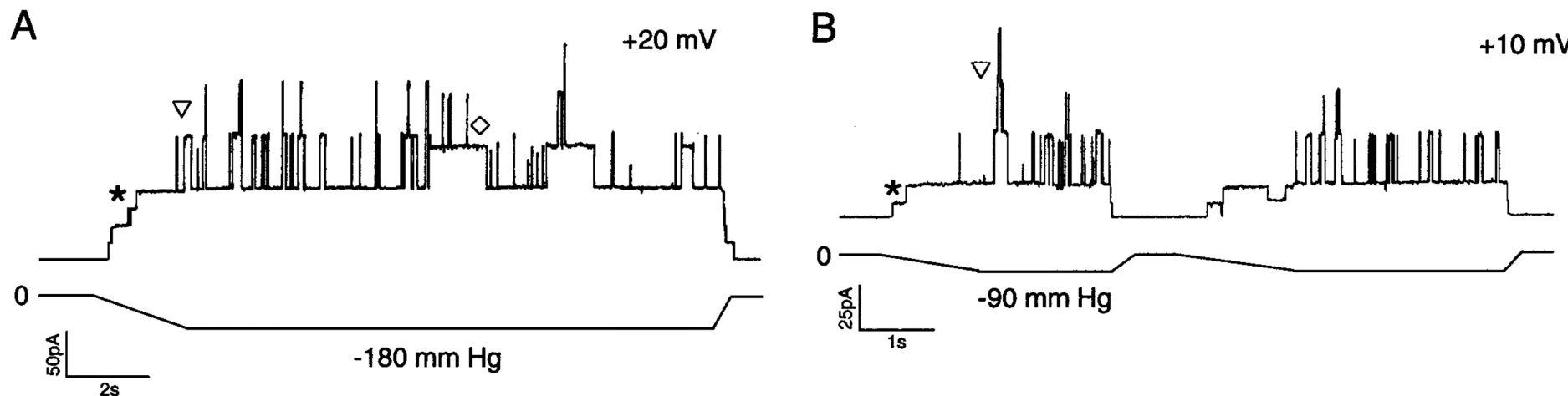
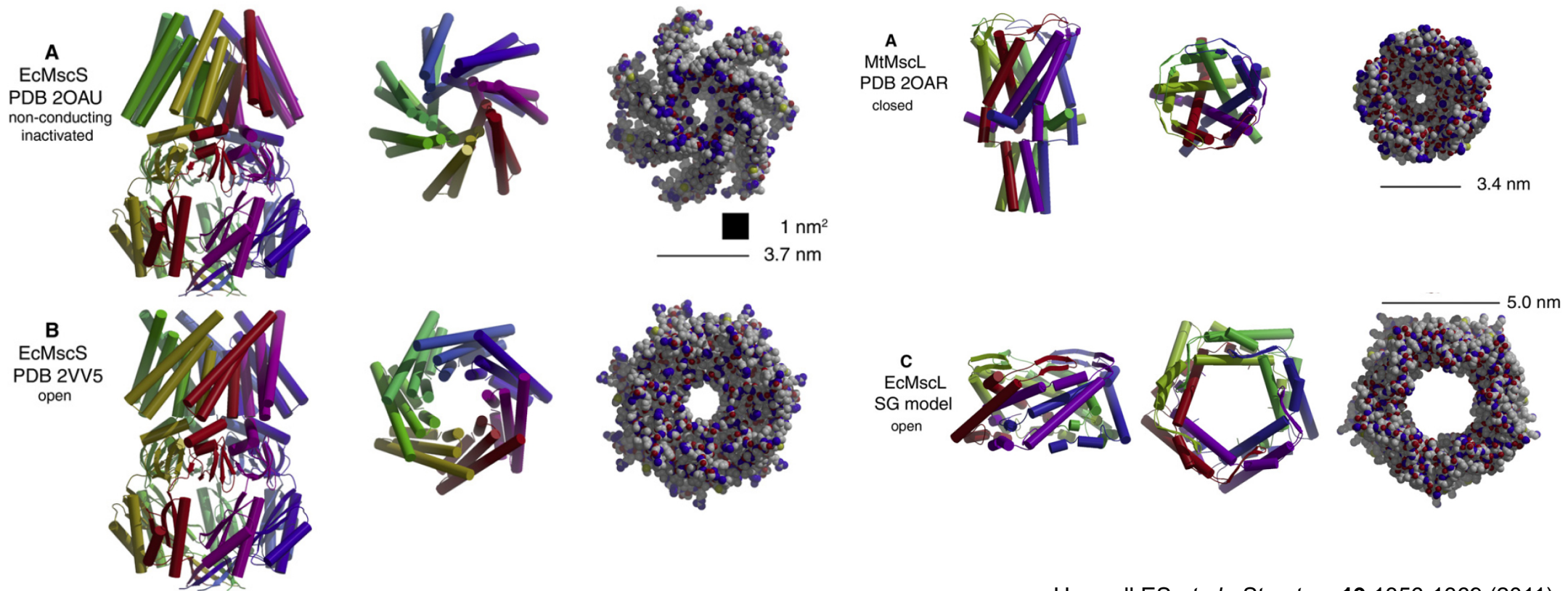


Figure 3 The two major *E. coli* MS channel activities and their separation by a sizing column. (A) The activities of MscL (triangle) and MscS (asterisk) recorded from a patch excised from a giant round-up cell, as diagrammed in Figure 1, second row. Note that MscS activities appear at lower suction than MscL activities. Substate behavior of MscL (diamond) is evident. (B) The same activities are observed in patches reconstituted with native-membrane vesicles as in Figure 1 (second row).

Structures of mechanosensitive channels MscL and MscS in closed and open conformations

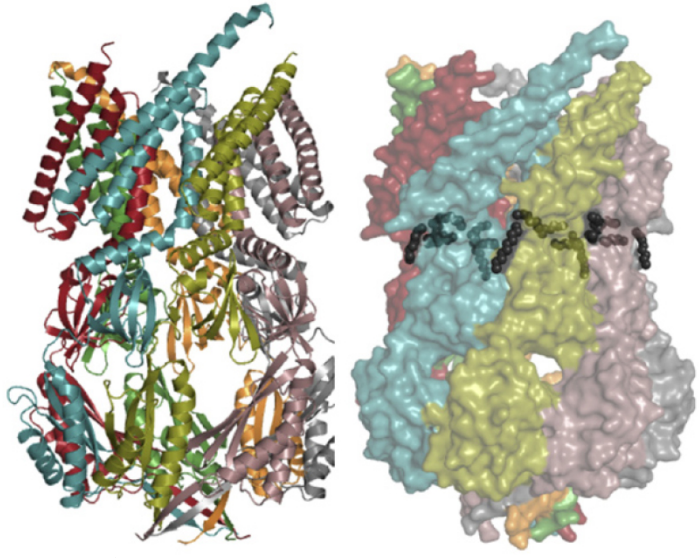


Douglas Rees

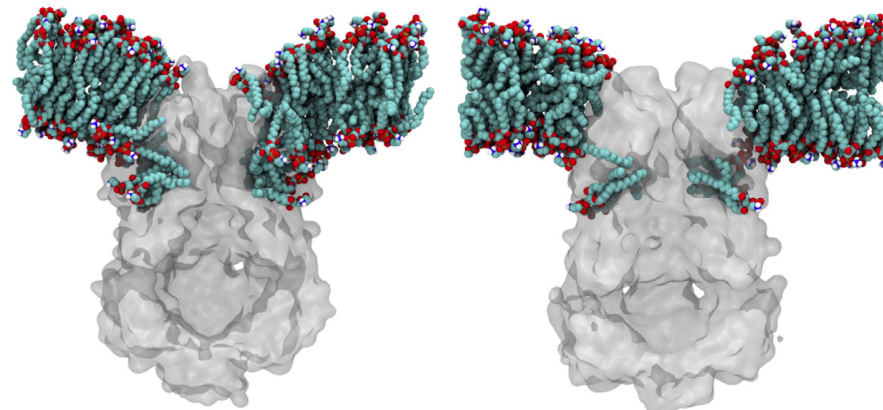


Haswell ES et al., *Structure* 19:1356-1369 (2011)

Mechanism of MscS – role of lipids in channel opening and closing



Left, 3.0 Å structure of D67R1 MscS heptamer. Right, surface model showing alkyl chains of bound lipids.



Ian Booth



James Naismith

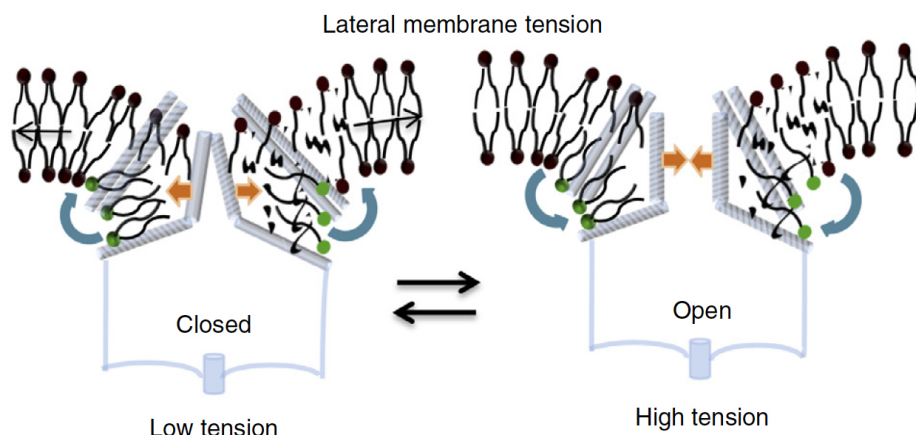
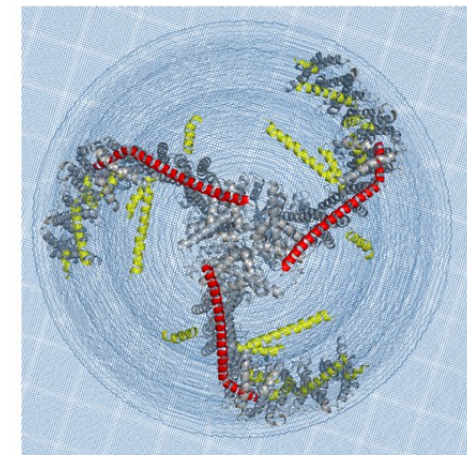
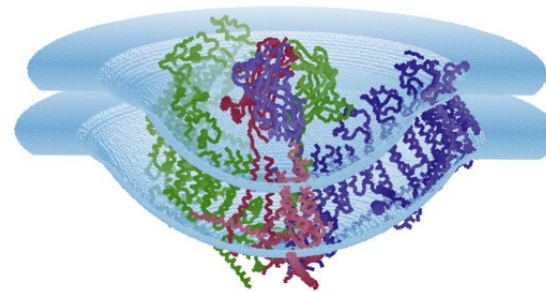
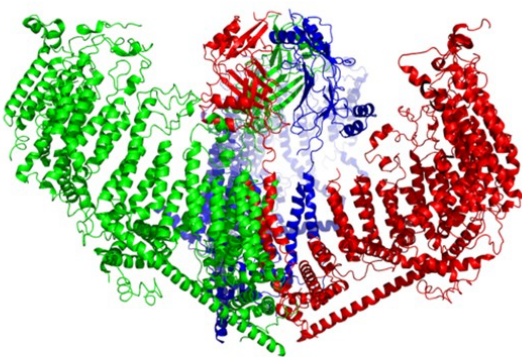
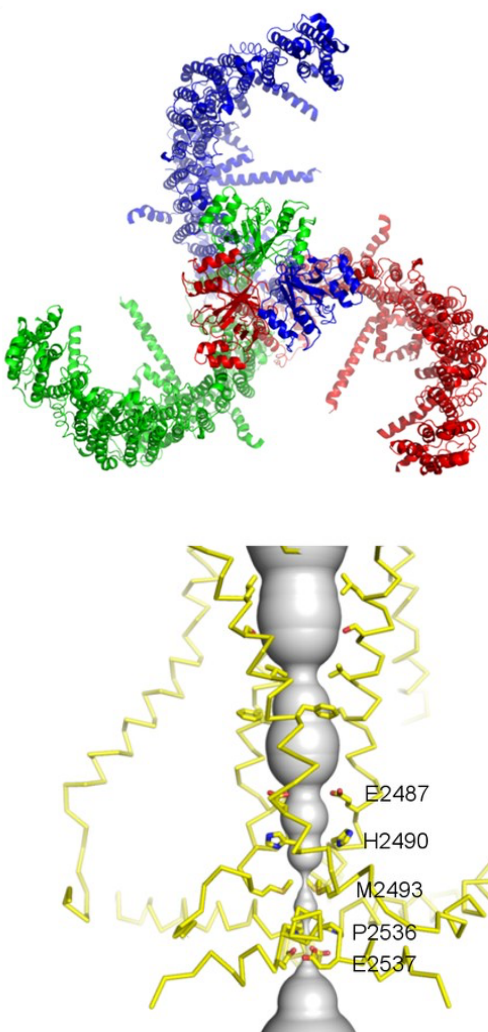


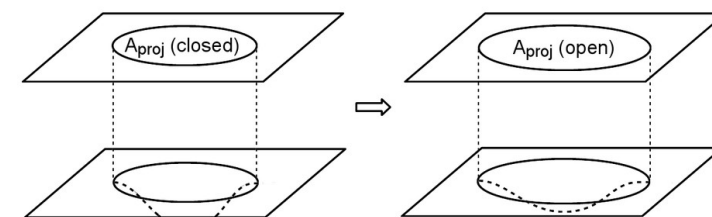
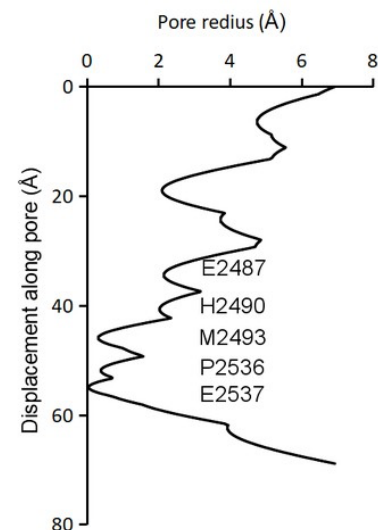
Figure 5 A model for mechanosensation. (a) The phospholipids partition in the pockets and the lipid bilayer. As pressure is applied, the lateral tension increases, and as a result the phospholipids repartition (blue arrows) from the protein pockets to the bilayer, thus destabilizing the closed structure. The protein responds by undergoing a conformational change (orange arrow) to the open form. MscS is depicted as a simplified line diagram. PE and PG molecules are shown with black head groups, and those inside the pockets are highlighted with a green head group.

Pliotas C et al., *Nat Struct Mol Biol* 22: 991-998 (2015)

Piezo channels: mechano-sensitive channels facilitating force detection



Guo YR, Mackinnon R, *Elife* 6: e33660 (2017)



Abstract Mechanosensitive ion channels convert external mechanical stimuli into electrochemical signals for critical processes including touch sensation, balance, and cardiovascular regulation. The best understood mechanosensitive channel, Mscl, opens a wide pore, which accounts for mechanosensitive gating due to in-plane area expansion. Eukaryotic Piezo channels have a narrow pore and therefore must capture mechanical forces to control gating in another way. We present a cryo-EM structure of mouse Piezo1 in a closed conformation at 3.7 \AA -resolution. The channel is a triskelion with arms consisting of repeated arrays of 4-TM structural units surrounding a pore. Its shape deforms the membrane locally into a dome. We present a hypothesis in which the membrane deformation changes upon channel opening. Quantitatively, membrane tension will alter gating energetics in proportion to the change in projected area under the dome. This mechanism can account for highly sensitive mechanical gating in the setting of a narrow, cation-selective pore.